THE EUROPEAN
PHYSICAL JOURNAL B

Regular Article

Linear-T scattering and pairing from antiferromagnetic fluctuations in the $(TMTSF)_2X$ organic superconductors

N. Doiron-Leyraud[1,a], S. René de Cotret[1], A. Sedeki[1], C. Bourbonnais[1], L. Taillefer[1], P. Auban-Senzier[2,b], D. Jérome[2], and K. Bechgaard[3]

1 Département de Physique and RQMP, Université de Sherbrooke, Sherbrooke, Québec, J1K 2R1, Canada
2 Laboratoire de Physique des Solides, UMR 8502 CNRS Université Paris-Sud, 91405 Orsay Cedex, France
3 Department of Chemistry, H.C. Ørsted Institute, Copenhagen, Denmark

Abstract. An exhaustive investigation of metallic electronic transport and superconductivity of organic superconductors $(TMTSF)_2ClO_4$ and $(TMTSF)_2PF_6$ in the pressure-temperature phase diagram between $T = 0$ and 20 K and a theoretical description based on the weak coupling renormalization group method are reported. The analysis of the data reveals a high temperature domain ($T \approx 20$ K) in which a regular T^2 electron-electron Umklapp scattering obeys a Kadowaki-Woods law and a low temperature regime ($T < 8$ K) where the resistivity is dominated by a linear-in temperature component. In both compounds a correlated behavior exists between the linear transport and the extra nuclear spin-lattice relaxation due to antiferromagnetic fluctuations. In addition, a tight connection is clearly established between linear transport and T_c. We propose a theoretical description of the anomalous resistivity based on a weak coupling renormalization group determination of electron-electron scattering rate. A linear resistivity is found and its origin lies in antiferromagnetic correlations sustained by Cooper pairing via constructive interference. The decay of the linear resistivity term under pressure is correlated with the strength of antiferromagnetic spin correlations and T_c, along with an unusual build-up of the Fermi liquid scattering. The results capture the key features of the low temperature electrical transport in the Bechgaard salts.

1 Introduction

A recent extensive study of the transport properties has been carried on in the most popular organic superconductors namely the Bechgaard salts, $(TMTSF)_2PF_6$ [1] and $(TMTSF)_2ClO_4$ [2] as a function of pressure [3,4]. This previous study has focused on the electronic transport at low temperature in the limit $T \rightarrow 0$ revealing the existence of a linear temperature dependence of the resistivity *at variance* with the sole T^2 dependence expected from the electron-electron scattering in a conventional Fermi liquid. Furthermore, the study has established a correlation between the amplitude of the prefactor A of the linear temperature dependence of the resistivity observed at low temperature and the value of the superconducting critical temperature T_c. Such a correlation between A and T_c has suggested in turn a common origin for the scattering and pairing in $(TMTSF)_2PF_6$ [5], both rooted in the low frequency antiferromagnetic fluctuations, as detected by NMR experiments [6–8]. Hence, the superconducting phase of $(TMTSF)_2PF_6$ might be controlled by

AF fluctuations with high pressure acting on the strength of correlations.

A preliminary extension of the transport analysis up to higher temperatures ($\approx$30 K) in $(TMTSF)_2PF_6$ [4] has suggested that the linear law is actually the low temperature limit of a more complex behaviour. In addition, reference [3] has pointed out a close correlation between the anomalous resistivity and the existence of an enhanced nuclear relaxation due to antiferromagnetic fluctuations. Although transport experiments had also been undertaken on $(TMTSF)_2ClO_4$, the ambient pressure analogue of $(TMTSF)_2PF_6$, leading to somewhat similar conclusions [5] a detailed analysis of the data is still missing. It is the goal of the present work.

While considered as belonging to the same family of organic superconductors, $(TMTSF)_2ClO_4$ is different from $(TMTSF)_2PF_6$ in some respects. It is already known from previous studies that superconductivity (SC) in $(TMTSF)_2ClO_4$ can be suppressed either by pressure [9] or by a controlled amount of non magnetic defects provided by alloying or residual disorder of non spherical ClO_4 anions [10,11].

The proximity between SC and SDW states is well established in the P-T phase diagram of $(TMTSF)_2PF_6$

a e-mail: ndl@physique.usherbrooke.ca
b e-mail: senzier@lps.u-psud.fr

and a SDW phase exhibiting insulating properties can also be stabilized in $(TMTSF)_2ClO_4$ under ambient pressure provided the sample is cooled fast enough to fulfill the so called quenched condition [12,13]. Given the similarities and the differences between $(TMTSF)_2ClO_4$ and $(TMTSF)_2PF_6$ regarding the problem of anions which is relevant in $(TMTSF)_2ClO_4$ only, it is important to analyze using the transport data, the roles of correlations (or pressure) and anions acting as parameters controlling the stability of SC in $(TMTSF)_2ClO_4$.

Electrical transport studies were paralleled and preceded on the theoretical side by a number of analysis making use of the weak coupling renormalization group (RG) approach to the description of the Bechgaard salts series [14–16]. In the framework of the quasi-one-dimensional electron gas model [17], these investigations provide a rather coherent picture of the mechanisms of instability of the metallic state toward the onset of long-range order in these materials. The RG calculations performed at the one-loop level showed that density-wave and Cooper pairings do not act as separate entities in perturbation theory. They mix and interfere at every order, a reciprocity of many-body processes that reproduces the SDW-SC sequence of instabilities in the P-T phase diagram of $(TMTSF)_2X$ under pressure. The same model proved to be also successful in describing the anomalous temperature dependence of the nuclear spin relaxation rate [8], T_1^{-1}, which stands out as a common characteristic of these materials above T_c [6,7]. It provided a microscopic explanation of the Curie-Weiss enhancement of T_1^{-1} [18], in terms of SDW fluctuations fueled by Cooper pairing in the metallic phase, linking then the size of T_c to the amplitude of spin fluctuations under pressure.

The extent to which the physics of the very same model and approach can throw light on the origin of non Fermi liquid electron transport above T_c, constitutes a clear-cut objective for the theory. A key ingredient for resistivity is the electron-electron scattering rate on the Fermi surface, a quantity that can be extracted from the calculation of the one-particle self-energy. It requires an extension of the RG method up to the two-loop level, a program that has been carried out recently [19]. The results will be used in a calculation of resistivity and their applicability to electrical transport experiments for $(TMTSF)_2PF_6$ and $(TMTSF)_2ClO_4$ attested.

2 Experimental

In the present paper we report on measurements of the electrical resistivity in $(TMTSF)_2ClO_4$ and $(TMTSF)_2PF_6$ mostly along the a-axis i.e, along the chains of organic molecules, as a function of pressure and temperature. Single crystals were grown by the usual method of electrocrystallisation [20]. Typical sample dimensions are $1.5 \times 0.2 \times 0.05$ mm^3 which are the length, width and thickness along the a, b, and c crystallographic axes, respectively. Electrical contacts were made with evaporated gold pads (typical resistance between 1 and

10 Ω) to which 17 μm gold wires were glued with silver paint. The current was applied along the a-axis. The magnetic field was aligned with the $c^\star$-axis. The electrical resistivity was measured with a resistance bridge using a standard four-terminal AC technique. Low excitation currents of typically 30 μA were applied in order to eliminate heating effects caused by the contact resistances. The samples used have typical values of a-axis conductivity near 500 $(\Omega$ cm$)^{-1}$ and 400 $(\Omega$ cm$)^{-1}$ for $(TMTSF)_2ClO_4$ and $(TMTSF)_2PF_6$ respectively. A non-magnetic piston-cylinder pressure cell was employed [21], with Daphne oil as pressure transmitting medium. The pressure at room temperature and 4.2 K was measured using the change in resistance and superconducting T_c of a Sn sample, respectively. Only the values recorded at 4.2 K are quoted here. The low temperature down to 0.1 K was provided by a demagnetization fridge. From room temperature down to 77 K the cooling rate was kept below 1 K/min to ensure gradual freezing of the pressure medium and an optimal level of pressure homogeneity, and to avoid the appearance of cracks in our samples. All the data reported here are on samples that showed no sign of cracks, i.e., their resistance at room temperature always recovered their initial value prior to each cooling cycle. No cracks were detected during pressurization either, i.e., the resistance at room temperature evolved smoothly with the applied pressure. Below 77 K, the cooling rate was kept below 5 K/h to ensure adequate thermal equilibrium between the samples and the temperature sensors placed outside the cell as slow cooling is vital to optimize anion ordering which occurs at 25 K at low pressure in $(TMTSF)_2ClO_4$.

3 Results

3.1 SC phase diagram

The superconducting transition temperature T_c was determined using the onset temperature according to the measured temperature dependence of the resistivity down to 0.1 K. Using such a determination for the onset of SC in transport data, the P-T superconducting phase diagram has been obtained as displayed in Figure 1a for $(TMTSF)_2PF_6$ and Figure 1b for $(TMTSF)_2ClO_4$. Note that the definition of T_c used in the present article, as the onset of the resistive transition, is different from that used in references [3,5], where T_c was defined as the midpoint of the resistive transition (i.e. mid-height of drop; see Fig. S9 in Ref. [5]). As a result, the present T_c values are slightly higher. Also, while for $(TMTSF)_2ClO_4$ T_c (midpoint) $\to 0$ at $P \approx 8$ kbar in reference [5], and for $(TMTSF)_2PF_6$ T_c (midpoint) $\to 0$ at $P \approx 22$ kbar in references [3,5], here we find T_c (onset) $\to 0$ at $P \approx 10$ kbar in $(TMTSF)_2ClO_4$ (Fig. 1b) and at $P > 24$ kbar in $(TMTSF)_2PF_6$ (Fig. 1a). As far as $(TMTSF)_2PF_6$ is concerned, the coexistence region between SDW and SC is well documented and a quantum critical point for the suppression of antiferromagnetic ordering would be located at 9.4 kbar with the present pressure scale [22,23].
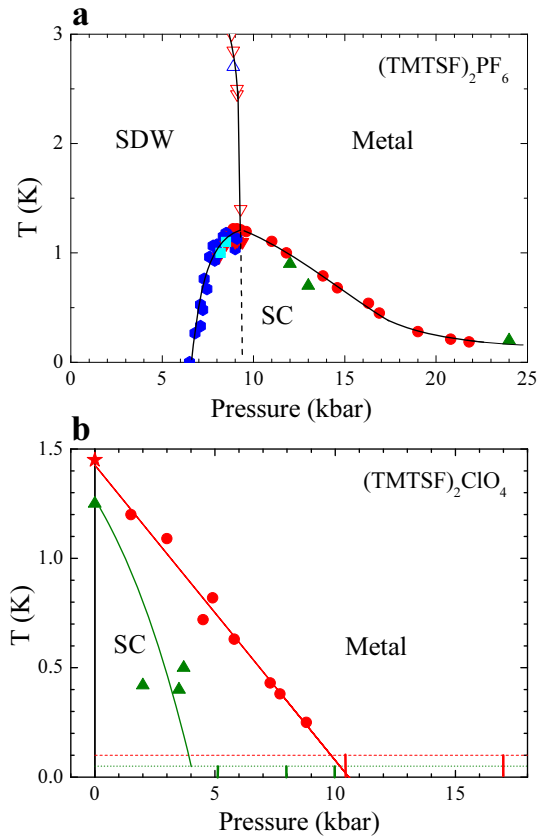
a

b

Fig. 1. (Color online) (a) (P-T) phase diagram of (TMTSF)$_2$PF$_6$ deduced from resistivity measurements. The data points below 9.4 kbar (the coexistence regime) are deduced from measurements along the three crystallographic axes: down triangles for ρ_a, squares for ρ_b, hexagons for ρ_c, empty symbols for T_{SDW} and full symbols for T_{SC} [22,23]. Above the critical pressure (9.4 kbar), only longitudinal resistivity data are plotted: (red) circles from this work and (green) triangles from reference [24]. (b) Pressure dependence of the superconducting transition of (TMTSF)$_2$ClO$_4$ deduced from longitudinal resistivity measurements: (red) circles from this work (the star at 1 bar is derived from a ρ_c measurement [25]) and (green) triangles from reference [9]. Dashed-dotted horizontal lines (red or green) indicate the lowest reached temperature without superconductivity for both studies. The (red) continuous line is a linear fit of the data including the point at 1 bar. T_c for (TMTSF)$_2$PF$_6$ although strongly decreasing under pressure does not reveal any critical pressure for the suppression of superconductivity *at variance* with (TMTSF)$_2$ClO$_4$ in which no T_c can be detected at 10.4 and 17 kbar. Such a different behavior can be ascribed to the pair breaking effect of residual anion disorder in (TMTSF)$_2$ClO$_4$ under pressure [26].

For (TMTSF)$_2$ClO$_4$ at ambient pressure, we took the value of T_c obtained from a good quality run performed on a ρ_c sample and cooled down to low temperature without any cracks [25]. All data points plotted as red circles in Figure 1 are obtained in the present work and are deduced from successive runs performed on the same sample of either (TMTSF)$_2$PF$_6$ or (TMTSF)$_2$ClO$_4$. Figure 1 deserves several comments as far as (TMTSF)$_2$ClO$_4$ is
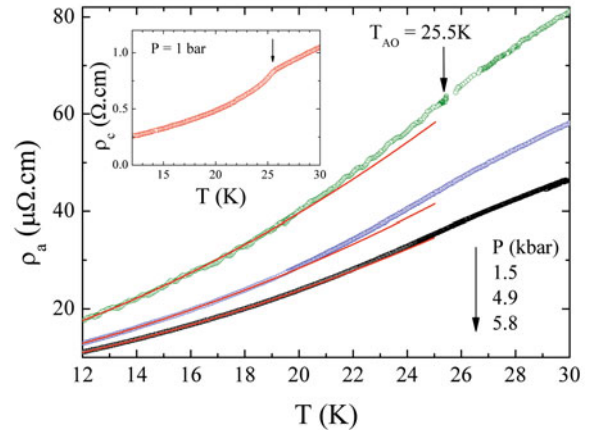

Fig. 2. (Color online) Temperature dependence of the longitudinal resistivity of (TMTSF)$_2$ClO$_4$ in the vicinity of the anion ordering, T_{AO}, for different applied pressures; insert: temperature dependence of the transverse resistivity of (TMTSF)$_2$ClO$_4$ at ambient pressure in the same temperature range [27].

concerned. The most significant one is the pressure dependence of T_c which deviates strongly from the previously published results [9]. As one cannot argue for real differences in the sample quality, all samples coming from the same chemistry lab, the difference between the two sets of data has to be found in a more intrinsic reason namely, the possible disorder introduced by ClO$_4$ anions on cooling.

There have been several reports related to the ordering of the anions in (TMTSF)$_2$ClO$_4$ [28–30]. First, fast cooling (quenching) of the sample is known to preclude the ordering of the anions. Instead of a SC ground state, it is a SDW insulating state which becomes the stable ground state below 5 K [12,31]. Second, the signature of the anion ordering on transport amounts to a drop of the resistivity at the ordering temperature T_{AO}, which also coincides with the onset of the superstructure observed in X-ray diffuse scattering experiments [28]. Furthermore, quench experiments suggest that the dynamics of anion orientation is rather slow at low temperature although this feature has yet to be studied more quantitatively under pressure [12,32].

A clear signature for the effect of anion ordering on the resistivity is provided by the transport under ambient pressure for ρ_c [27], see insert of Figure 2, and under $P = $ 1.5 kbar for ρ_a (see Fig. 2).

The ordering of the anions decreases the amount of static disorder and in turn the strength of elastic scattering of the carriers, as it can be seen by a drop of the resistivity below T_{AO}; this amounts to about $\Delta\rho \approx 100$ mΩ cm and 2–3 mΩ cm for transverse and longitudinal transports respectively, see Figure 2.

In the present pressure study, special attention has been paid to the cooling conditions in order to guarantee the best possible anion ordering. As seen in Figure 2, a broad shoulder, although smaller in amplitude than the ambient pressure one, is still observed up to 5.8 kbar at a temperature of about 25.5 K, which can be attributed

to the signature of an anion ordering still present under pressure. Our results do show that T_{AO} persists above 1.5 kbar and then becomes hardly affected by pressure. This feature corroborates previous pressure experiments showing that above the low pressure regime where the initial pressure dependence of T_{AO} is large, the pressure coefficient becomes much smaller [33–35]. An opposite conclusion namely, the anion ordering is suppressed under pressure, had been claimed according to a study of the angular magnetoresistance [36] .

However, it looks as if long-range ordering becomes less perfect at low temperature under pressure since the amplitude of the drop of the resistivity is seen to decrease under pressure [35]. Consequently, the anion ordering possibly spreads over a broader temperature regime below T_{AO}. We suggest that this can be a result of anion dynamics slowing down under pressure [35].

Hence, we propose that the P-T phase diagram of $(TMTSF)_2ClO_4$ shown in this work is the one relevant for samples exhibiting the highest possible degree of anion ordering namely, the same cooling rate in the vicinity of the anion ordering temperature as used in reference [35]. The difference between the present phase diagram and the one inferred from the data of 1985 can be attributed to cooling conditions not being slow enough in the early experiments. Actually, the effect of the cooling rate on T_c has been studied at ambient pressure in some details. Increasing the cooling rate prevents a good ordering of the ClO_4 anions and in turn depresses T_c. Above a rate of 15 K/mn, it is the SDW phase that becomes the stable ground state [12,37,38].

We see in Figure 1 that T_c for $(TMTSF)_2ClO_4$ varies linearly with pressure and its extrapolation hits the pressure axis around 10 kbar. In contrast, in $(TMTSF)_2PF_6$ a T_c of 0.2 K is still obtained under 24 kbar [39] i.e., 14–15 kbar beyond the critical pressure for the stabilization of SC. $(TMTSF)_2PF_6$ is a compound where the disorder of the anions does not come into play and therefore pressure is the only control parameter for SC as long as the samples do not suffer from chemical defects or other kinds of defects.

3.2 Transport

3.2.1 $(TMTSF)_2PF_6$

Figure 3a, displays a typical temperature dependence up to 20 K for the longitudinal resistivity of $(TMTSF)_2PF_6$ under 11.8 kbar, a pressure which is close to the critical pressure P_c. Data are shown at zero field and under $H = 0.05$ T along c^* in order to suppress SC without magnetoresistance. Below $P_c = 9.4$ kbar, $(TMTSF)_2PF_6$ still exhibits SC features but they arise in the coexistence regime below the onset of a SDW state [23] which is not relevant for the present study.

The important feature emerging from the resistivity data in Figure 3a is the linear temperature dependence below 8 K, becoming quadratic at higher temperatures. This quadratic contribution is absent at low temperature while
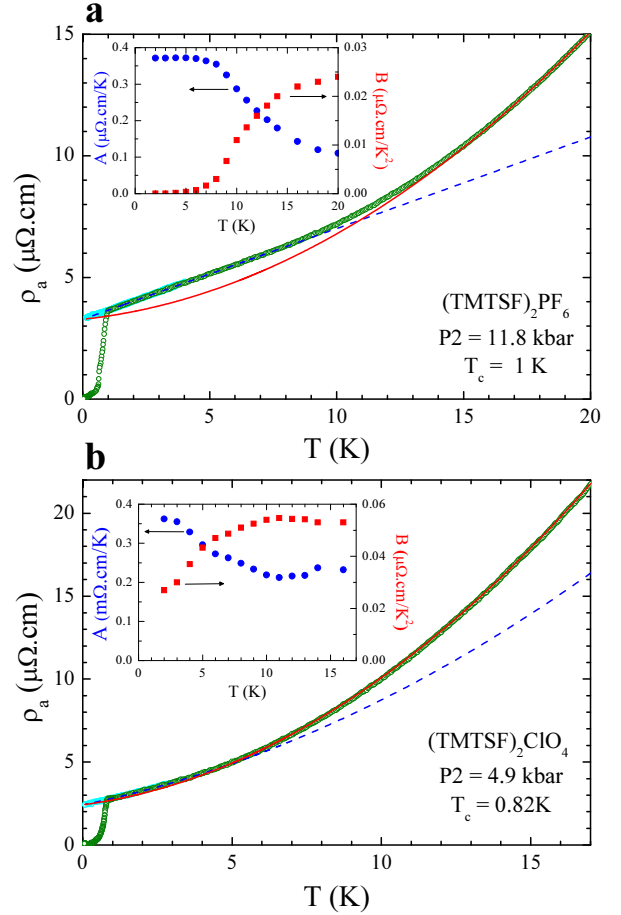

Fig. 3. (Color online) Temperature dependence of the longitudinal resistivity of $(TMTSF)_2PF_6$ at $P = 11.8$ kbar below 20 K (a), and $(TMTSF)_2ClO_4$ at $P = 4.9$ kbar below 17 K (b), at zero field and under $H = 0.05$ T along c^* in order to suppress SC. The second order polynomial fit, $\rho(T) = \rho_0 + A(T)T + B(T)T^2$, according to the sliding fit procedure described in the text is shown for the T intervals $(2-6)$ K and $(18-22)$ K or $(13-17)$ K in blue and red respectively. The top inserts provide the temperature dependence of the A and B coefficients.

the linear one becomes weaker at high temperature. Although the linear behaviour is the dominant feature of the resistivity at low temperature, a small saturation becomes observable below 2 K at pressures much higher than P_c.

Taking into account these two contributions to the resistivity we have analyzed the transport in $(TMTSF)_2PF_6$ fitting the experimental data in the normal state (both at zero field and under a small magnetic field) by a second order polynomial form such as $\rho(T) = \rho_0 + A(T)T + B(T)T^2$. Here, both A and B prefactors can be temperature dependent, while the value of ρ_0 depends on pressure only. The residual resistivity ρ_0 is first extracted from the fit between 0.1 and 4 K. For the determination of A and B a fit of the experimental data is performed at the temperature T over a temperature window of 4 K centered on T, keeping the same value for ρ_0. The present analysis is restricted to the temperature domain below 20 K because
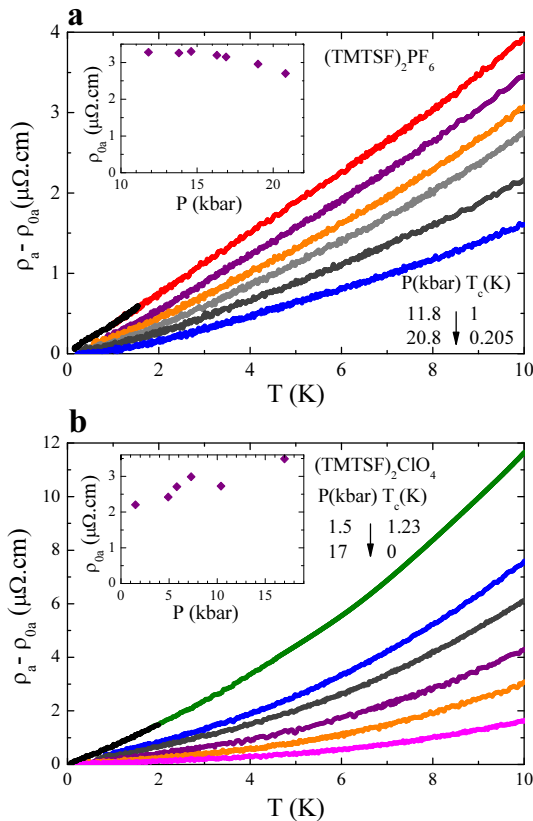
Fig. 4. (Color online) Inelastic contribution $\rho_a - \rho_{0a}$ of the normal state resistivity at different pressures for $(TMTSF)_2PF_6$ (a) and $(TMTSF)_2ClO_4$ (b). Data under a small magnetic field (black) are shown for the lowest pressure only. Inserts show the pressure dependence of the residual resistivity, ρ_{0a}, deduced from the low temperature fit.

measurements of the transverse transport in the same materials [27] have shown that a cross-over from coherent to incoherent transverse transport along $c^\star$ is occurring at higher temperatures. This may in turn affect the temperature dependence of the longitudinal resistivity since a logarithmic factor should be added to the quadratic law in the two dimensional regime when neighboring (a, b) planes are decoupled [27,40,41].

The result of this analysis at 11.8 kbar is displayed on the insert of Figure 3a namely, a coexistence of the A and B contributions to the transport over the whole temperature domain with a predominance for the linear contribution over the quadratic one at low temperature and the reverse at high temperature.

Similar analysis have subsequently been conducted on transport data performed on the same sample under seven pressures (11.8, 13.8, 14.6, 16.3, 16.9, 19 and 20.8 kbar). The inelastic resistivity data are displayed in Figure 4a and the results for for $A(T)$ and $B(T)$ shown in Figure 5a after the determination of the residual resistivity under every pressure.

The pressure dependence of the residual resistivity displayed in the insert of Figure 4a shows a smooth and weak *decrease*. The smoothness of the pressure dependence of

ρ_0 is an indication for the reliability of the data of the seven successive pressure runs. The pressure coefficient (-2.5%/kbar) can be ascribed to the expected decrease of the effective mass under pressure [42,43]. The presence of a small saturation below 2 K manifests as a large increase of B below 5 K while at the same time A is slightly decreasing. This effect is relatively more pronounced for the highest pressures.

3.2.2 $(TMTSF)_2ClO_4$

A similar investigation has been performed on $(TMTSF)_2ClO_4$, although restricted to the pressure regime 1 bar–17 kbar since superconductivity is already stable at ambient pressure in this compound. A typical temperature dependence for ρ_a is shown in Figure 3b at the pressure of $P = 4.9$ kbar. For the analysis of the $(TMTSF)_2ClO_4$ data, using the same procedure as for $(TMTSF)_2PF_6$, we restrict ourselves to the temperature domain between 0.1 and 16 K since the actual temperature dependence above 16 K is affected by the extrinsic influence of anion ordering occurring around 25 K. Unlike $(TMTSF)_2PF_6$, the difference between low and high temperature regimes for $(TMTSF)_2ClO_4$ is not as pronounced. A significant quadratic contribution remains at low temperature besides the dominant linear one and no additional saturation could be detected at very low temperature. Effectively, the data for $(TMTSF)_2ClO_4$ at $P = 4.9$ kbar in Figure 3b reveal a resistivity which retains a finite temperature dependence approaching 0 K, but follows a quadratic dependence above 12 K or so. The analysis of the resistivity at $P = 4.9$ kbar according to the sliding fit procedure is shown in the insert of Figure 3b. The results of the analysis of five consecutive pressure runs (1.5, 4.9, 5.8, 7.3 and 10.4 kbar) over ten performed on the same sample are shown in Figure 4b for the inelastic contribution and in Figure 5b for the prefactors A and B. The smoothness of the variation of the residual resistivity *increasing* under pressure is also an indication for the good quality of the data. We can ascribe the slight increase of ρ_0 under pressure, instead of a decrease for $(TMTSF)_2PF_6$, to the anion ordering becoming less complete at T_{AO} under pressure and spreading all the way down to 0 K on account of the pressure-induced slowing down of the anion dynamics discussed above.

4 Discussion

4.1 Transport

4.1.1 The A contribution

Figure 6 shows that a correlation between A and T_c can be established in both compounds using A_{LT}, the maximum value of A determined at low temperature and T_c given by the onset of SC. For $(TMTSF)_2PF_6$, the maximum value
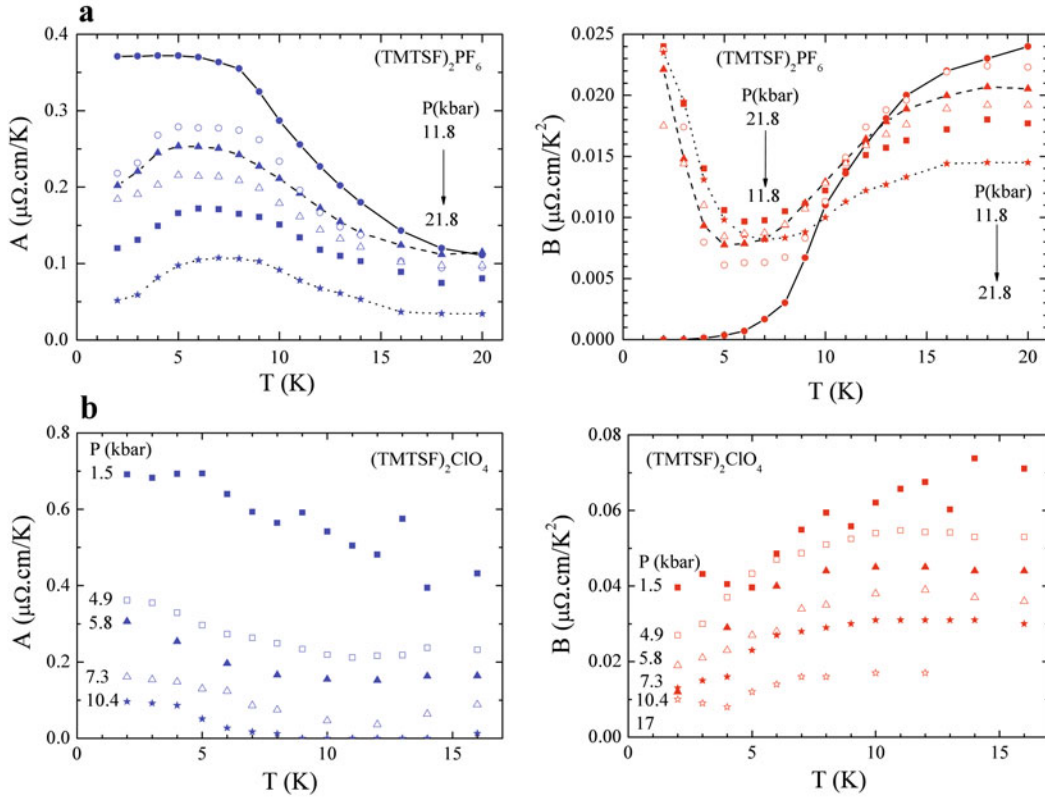
Fig. 5. (Color online) Temperature dependence of A (left) and B (right) coefficients of the polynomial fit, $\rho(T) = \rho_0 + AT + BT^2$ at different pressures for $(TMTSF)_2PF_6$ (a) and $(TMTSF)_2ClO_4$ (b). Each temperature point corresponds to the center of a 4 K window used for the fit. As far as $(TMTSF)_2PF_6$ is concerned, this figure shows that under 11.8 kbar B is zero and A constant below 4 K within the accuracy of the measurements and data processing. However, a small low temperature quadratic term arises at larger pressures, (see Fig. 7).

of A is reached at a temperature which is slightly increasing with pressure (from 4 K at 11.8 kbar up to 7 K at 20.8 kbar) while for $(TMTSF)_2ClO_4$, it is always reached at the lowest temperature (0.1–4 K window). As far as $(TMTSF)_2PF_6$ is concerned, the pressure dependence of both quantities are nearly parallel. SC is observed up to the maximum accessible pressure (20.8 kbar) and A_{LT} remains finite at such a pressure. The relation between A_{LT} and T_c under pressure is different in $(TMTSF)_2ClO_4$. Both quantities are quite parallel in the low pressure limit, but a finite value of A_{LT} persists even in the absence of SC under pressure as shown by the pressure runs at 10.4 and 17 kbar where no SC can be observed above 0.1 K *at variance* with $(TMTSF)_2PF_6$. Such differences between pressure dependences in these two organic superconductors can again be explained by the particular role played by the anions in case of $(TMTSF)_2ClO_4$ since the frozen anion disorder is affecting the stability of the superconducting phase but not the inelastic contribution to the transport. This hypothesis is supported by the investigation of SC in solid solutions $(TMTSF)_2ClO_{4(1-x)}ReO_{4x}$ when non magnetic point defects are introduced by alloying in a controlled way [11]. It can be ascribed to the pair breaking effect of non magnetic defects in a superconductor exhibiting line nodes in the gap [26].

4.1.2 The B contribution

Unlike A, no direct correlation can be established between B and T_c. The quadratic law is a well established behaviour in $(TMTSF)_2X$ below 50 K or so [44,45]. This law was noticed in the early studies of $(TMTSF)_2AsF_6$ under ambient pressure [46] and is still valid under 20.8 kbar in $(TMTSF)_2PF_6$. The same is true for $(TMTSF)_2ClO_4$ even under 10.4 and 17 kbar when no SC can be observed above 0.1 K. Furthermore, for both compounds an experimental correlation can be established between B and the electronic spin susceptibility. As shown in Figure 7a for $(TMTSF)_2PF_6$, the prefactor B_{HT} namely, B of the polynomial law taken at high temperature and the square of the electronic spin susceptibility given by the NMR relaxation rate data at high temperature ($\chi^2(q=0) \propto 1/T_1T$) [6] follow the same pressure dependence. This behaviour is actually reminiscent of the Kadowaki-Woods law observed in various strongly correlated metals [48,49]. Similar to A, the B contribution is not affected by impurities provided by alloying or by the frozen anion disorder [27]. B is controlled by pressure only. A similar comparison between B and the spin susceptibility under pressure is shown in $(TMTSF)_2ClO_4$ in Figure 7b. The quality of the agreement between NMR
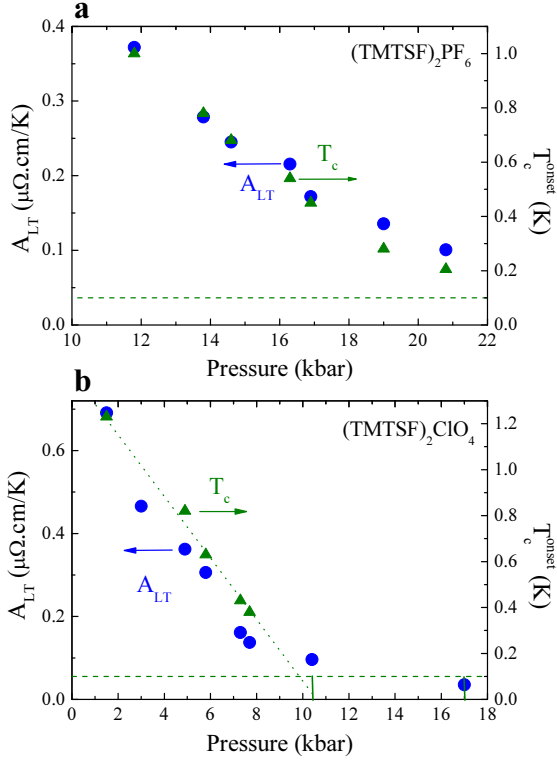
Fig. 6. (Color online) Pressure dependence of T_c onset and A_{LT} coefficient for $(TMTSF)_2PF_6$ (a) and $(TMTSF)_2ClO_4$ (b). A_{LT} is obtained from the second order polynomial fit described in the text in the temperature window corresponding to its maximum value for $(TMTSF)_2PF_6$ and in the $0.1-4$ K window for $(TMTSF)_2ClO_4$. The horizontal dashed lines indicate our lowest reached temperature, 0.1 K. For $(TMTSF)_2ClO_4$, the vertical lines below this temperature indicate the pressure points at 10.4 and 17 kbar without superconductivity and the dotted line is a linear fit of T_c onset data points.
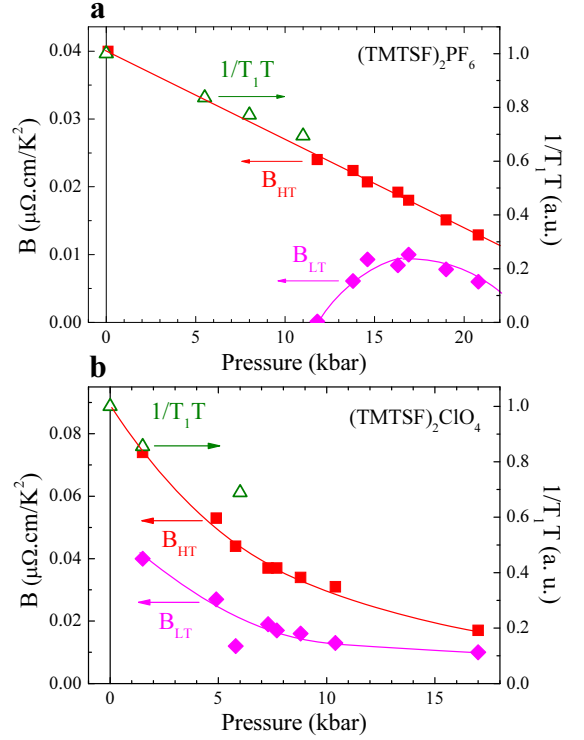

Fig. 7. (Color online) Pressure dependence of the B_{HT} coefficient, obtained from the high temperature ($T = 20$ K) polynomial fit, of the spin susceptibility measured under pressure via NMR relaxation experiments [16] ($\chi^2(q = 0) \propto 1/T_1T$) and of the B_{LT} coefficient, determined in the same temperature window as A_{LT} coefficient, for $(TMTSF)_2PF_6$ (a). The ambient pressure point for B_{HT} is deduced from a-axis resistivity data in reference [46]. Similar plot for $(TMTSF)_2ClO_4$ (b) using the NMR data from reference [47]. The relation $B \propto \chi^2$ is indicative of the Kadowaki-Woods relation encountered in strongly correlated metals [48].

and transport data is not as good for $(TMTSF)_2ClO_4$. This could be due to a large uncertainty in the knowledge of pressure at low temperature in this early NMR experiment [47] using argon as the pressure medium.

In addition, data of $(TMTSF)_2PF_6$ in Figure 5 reveal an interesting behaviour for B_{LT} in the low temperature domain. At 5 K, B_{LT} starting from a zero value under 11.8 kbar is increasing sharply at higher pressures and then levels off as displayed in Figure 7a. It is actually the reason for the observation of a linear resistance in $(TMTSF)_2PF_6$ when the pressure is close to the critical pressure. We may also notice that quite a similar behaviour has derived from the measurement of ρ_c at the same pressure although on different $(TMTSF)_2PF_6$ samples [27]. However, such a crossing in the temperature dependence of the B coefficients seen in Figure 5 is not observed in the $(TMTSF)_2ClO_4$ compound where B never reaches a zero value at low temperature even in the vicinity of ambient pressure. Figure 7b shows a parallel evolution with pressure for B_{LT} and B_{HT}. We may suggest several reasons for the difference between compounds. First,

the quadratic term is stronger in $(TMTSF)_2ClO_4$ than in $(TMTSF)_2PF_6$ possibly due to a transverse coupling $t_\perp$ being larger in the latter compound under pressure with $B \propto 1/t_\perp$ for a Q1D Fermi surface [40]. Second, the temperature dependence of ρ may be spoiled in $(TMTSF)_2ClO_4$ by the extended anion ordering occurring on cooling.

4.2 Interplay between transport and magnetism

The remarkable feature of the transport analyzed according to the procedure presented above up to 20 K is the temperature dependence of the prefactors in the temperature dependence of the resistivity when a second order polynomial form is assumed for its temperature dependence. The linear term was shown to be related to the scattering of the carriers off AF fluctuations [3] which are also active contributing to the nuclear spin-lattice relaxation adding a fluctuation contribution to the regular Korringa contribution [8] (see Sect. 5). A comparison between A and the extra relaxation from AF spin
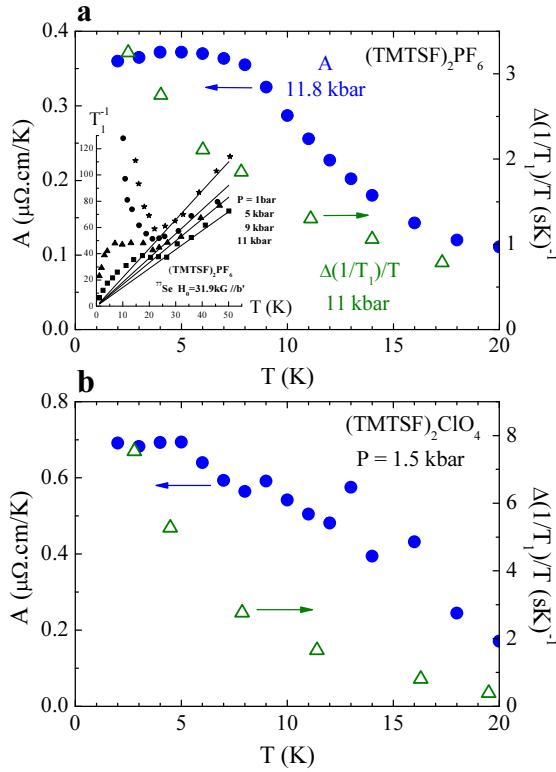
Fig. 8. (Color online) (a) Temperature dependence of the fluctuation-induced relaxation $\Delta(1/T_1)/T$ at 11 kbar deduced from NMR data in reference [16] and of the coefficient of the linear resistivity (A) at 11.8 kbar for $(TMTSF)_2PF_6$. The insert shows the ^{77}Se relaxation data at four different pressures where the bump of extra relaxation coming form AF fluctuations is clearly seen [16]. Similar results have been obtained in reference [7]. (b) Temperature dependence of the fluctuation-induced relaxation $\Delta(1/T_1)/T$ at a pressure of 5 kbar at room temperature, from reference [47], estimated to be around 1.5 kbar at low temperature, and of the coefficient of the linear resistivity (A) at 1.5 kbar for $(TMTSF)_2ClO_4$.

fluctuations, subtracting the Korringa relaxation from the experimental data is shown in Figure 8 for $(TMTSF)_2PF_6$ at 11 kbar (a) and for $(TMTSF)_2ClO_4$ around 1.5 kbar (b).

However, the comparison between temperature dependencies of A and $\Delta(1/T_1T)$ should not be taken at face value since transport and NMR experiments have been conducted at pressures of 11 and 11.8 kbar for NMR [16] and transport in $(TMTSF)_2PF_6$ respectively. It is only a confirmation for a common origin for the linear law in transport and the enhancement of relaxation due to the onset of AF fluctuations at low temperature. For both compounds the singular carrier scattering and AF fluctuations go hand in hand in temperature and also under pressure. It is tempting for $(TMTSF)_2PF_6$ to link the drop of the factor B_{LT} (related to the regular electron-electron Umklapp scattering), which is observed close to P_c (see Fig. 7a) to the opening of a pseudogap in the density of states related to fluctuations as observed in 1D

conductors with a Peierls ground state [50]. If this were the case, the amplitude for the residual resistivity coming from a fit of the high temperature quadratic regime with a constant plus a quadratic T dependent contribution should be smaller (and not larger as observed experimentally) than the value for the residual resistivity given by the procedure presented in this work. In addition, with the pseudogap scenario the residual resistivity should reveal a much stronger pressure dependence than what is actually observed in the insert of Figure 4a.

Moreover, as far as the spin sector is concerned, no gap opens in the same temperature range according to the Faraday susceptibility which is nearly temperature independent below 30 K in $(TMTSF)_2ClO_4$ [51,52] and also in NMR where relaxation data in $(TMTSF)_2PF_6$ do not reveal any precursor drop of the relaxation rate [6].

5 Theoretical aspects and connection to experiment

In this section we highlight some results of the renormalization group (RG) method obtained in the framework of the quasi-one-dimensional electron gas model. Their link with the properties of the Bechgaard salts and their applicability to the resistivity data of the preceding sections will be discussed.

5.1 Previous results: phase diagram and nuclear relaxation

The non interacting part of the quasi-one-dimensional electron gas model is defined in terms of a strongly anisotropic electron spectrum yielding an orthorhombic variant of the open Fermi surface in the ab plane of the Bechgaard salts. The spectrum $E(\mathbf{k}) = v_F(|k| - k_F) - 2t_\perp \cos k_\perp - 2t'_\perp \cos 2k_\perp$ as a function of the momentum $\mathbf{k} = (k, k_\perp)$ is characterized by an intrachain or longitudinal Fermi energy $E_F = v_F k_F$ which revolves around 3000 K in $(TMTSF)_2X$ [53,54]; here v_F and k_F are the longitudinal Fermi velocity and wave vector ($\hbar = 1$ and $k_B = 1$ throughout this section). This energy is much larger than the interchain hopping integral $t_\perp$ ($\approx$200 K), in turn much bigger than the second-nearest neighbor transverse hopping amplitude $t'_\perp$. The latter stands as the antinesting parameter of the spectrum which simulates the main influence of pressure in the model. The interchain hopping in the third and less conducting direction is neglected. Electrons pertaining to different Fermi sheets are interacting through the backward and forward scattering amplitudes g_1 and g_2, to which small longitudinal Umklapp scattering term $g_3 \ll g_1$, is added as a consequence of the slight dimerization of the stacks and the anion potential [17]; here all interactions are normalized by the bandwidth $2E_F = \pi v_F$.

The interaction parameters that shall be used in the following coincide with those previously employed in the RG description of the phase diagram and NMR spin-lattice relaxation rate [8,15]. Taking $g_1 = g_2/2 \approx 0.32$ and
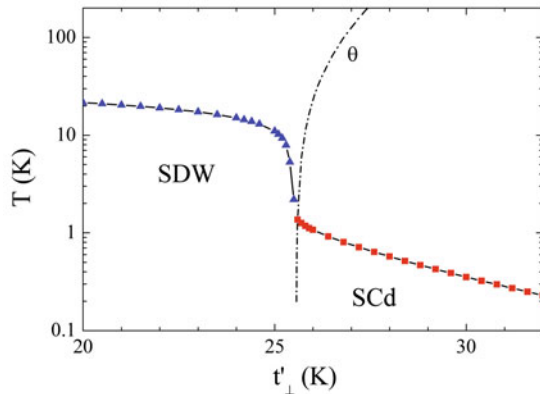
Fig. 9. (Color online) Calculated phase diagram of the quasi-one-dimensional electron gas model. The scale Θ (dashed line) is the Curie-Weiss temperature

$g_3 \approx 0.02$, the RG integration of high energy electronic degrees of freedom is carried out down to the Fermi level, which leads to the flow or renormalization of the couplings at the temperature T [8,14,15]. At the one-loop level, the flow superimposes the $2k_F$ electron-hole (density-wave) and Cooper pairing many-body processes which combine and interfere at every order of perturbation. As a function of the 'pressure' parameter $t'_\perp$, a singularity in the scattering amplitudes signals an instability of the metallic state toward the formation of an ordered state at some characteristic temperature scale. At low $t'_\perp$, nesting is sufficiently strong to induce an SDW instability in the temperature range of experimental $T_{SDW} \sim 10-20$ K. When the antinesting parameter approaches the threshold $t'^*_\perp$ from below ($t'^*_\perp \approx 25.4$ K, using the above parameters), T_{SDW} sharply decreases and as a result of interference, SDW correlations ensure Cooper pairing attraction in the superconducting d-wave (SCd) channel. This gives rise to an instability of the normal state for the onset of SCd order at the temperature T_c. The maximum $T_c \approx 1.4$ K is reached at $t'^*_\perp$, where a steady decline is initiated as $t'_\perp$ is further increased. The calculated scale for ordering yields the phase diagram of Figure 9, which reproduces the experimental trace for the onset of long-range ordering in a system like (TMTSF)$_2$PF$_6$ (Fig. 1). Another peculiar feature that comes out of the calculations concerns the enhancement of spin correlations above T_c. It has been shown that despite strong alterations of the nesting conditions and the existence of a singlet SCd ground state, the SDW susceptibility continues to grow as the temperature is lowered following a Curie-Weiss law $\chi_{SDW} \sim \xi^2$ where $\xi \propto (T + \Theta)^{-1/2}$ is the SDW correlation length [8]. This behavior reveals the constructive feedback of Cooper pairing on antiferromagnetism, as mentioned above. The Curie-Weiss scale $\Theta \to 0$ is critical at $t'^*_\perp$, whereupon it undergoes a rapid increase with $t'_\perp$ (Fig. 9). Because of the onset of superconductivity at T^*_c, however, the quantum critical behavior of $\chi_{SDW} \sim 1/T$ is avoided at $t'^*_\perp$ [8].

The Curie-Weiss behavior has been shown to also govern the enhancement of the nuclear relaxation rate T_1^{-1} by SDW fluctuations. Deviations to the Korringa law take the form $(T_1 T)^{-1} \sim (T + \Theta)^{-1}$ at low temperature [8], in accordance with the experimental results for (TMTSF)$_2$PF$_6$ [7,18,55] (inset of Fig. 7) and (TMTSF)$_2$ClO$_4$ [47,56,57]. The pressure dependence of Θ for both compounds is consistent with a critical reduction of this scale as $P \to P_c$, namely when T_c reaches its maximum value (Fig. 1a).

5.2 Quasi-particle scattering rate and resistivity

The impact that can have the correlations responsible of the structure of the phase diagram and the anomalous nuclear relaxation on the single particle properties can be examined by performing the RG procedure at the two-loop level. In reference [19], one-particle self-energy RG calculations have been carried out using for the vertex part the contributions of the mixed electron-electron and electron-hole scattering channels obtained in the one-loop level. Thus the calculation of the one-particle Matsubara self-energy, $\Sigma_s(\mathbf{k}_F(k_\perp), i\omega_n)$, allows us to extract the electron-electron scattering rate at $\mathbf{k}_F(k_\perp)$ on the Fermi surface. The Fermi wave vector $\mathbf{k}_F(k_\perp)$ is parametrized by the transverse wave vector $k_\perp$. The scattering rate is obtained by the analytic continuation of $\Sigma_s(\mathbf{k}_F(k_\perp), i\omega_n)$ to the so-called retarded form $\Sigma_s(\mathbf{k}_F(k_\perp), \omega + i0^+)$ defined on the real ω axis, and which consists of a real (Σ'_s) and imaginary (Σ''_s) parts. From the zero frequency limit of the imaginary part, one defines the decay rate of quasi-particles on the Fermi surface $\tau_{k_\perp}^{-1} \equiv -2\Sigma''_s(\mathbf{k}_F(k_\perp), \omega \to 0)$.

In the metallic state of the superconducting sector $t'_\perp > t'^*_\perp$ of the phase diagram shown in Figure 9, the scattering rate turns out to be anomalous in both $k_\perp$ and T [19]. Marked deviations with respect to the Fermi liquid behavior $\tau_{k_\perp}^{-1} \sim T^2$ are found, deviations whose amplitude strongly varies with $k_\perp$. The absolute maximum is found in the longitudinal direction $k_\perp = 0$, with secondary maxima taking place at $k_\perp = \pm\pi$, namely where the edges of the open Fermi surface cross the Brillouin zone in the perpendicular direction. These points markedly differ from the expected 'hot' spots at $k_\perp = \pm\pi/4$ and $\pm 3\pi/4$, as deduced from $E(\mathbf{k})$ at the best nesting conditions for the antiferromagnetic wave vector $\mathbf{q}_0 = (2k_F, \pi)$. The anisotropy results from the interference of electron-hole with electron-electron scattering, which moves the maxima in the regions where the superconducting SCd order parameter or the gap is expected to take its largest values below T_c.

Assuming that correlations over which electrons scatter are at equilibrium and can degrade momentum through Umklapp or impurity scattering, the decay rate will also affect conductivity. In the relaxation time approximation, the contribution of the above singular part of the self-energy to the static conductivity at low temperature is given by

$$\sigma_s = \frac{\omega_p^2}{4\pi}\langle\tau_{k_\perp}\rangle, \tag{1}$$

where $\langle\tau_{k_\perp}\rangle$ stands as the average of the relaxation time over the Fermi surface and ω_p is the longitudinal plasma
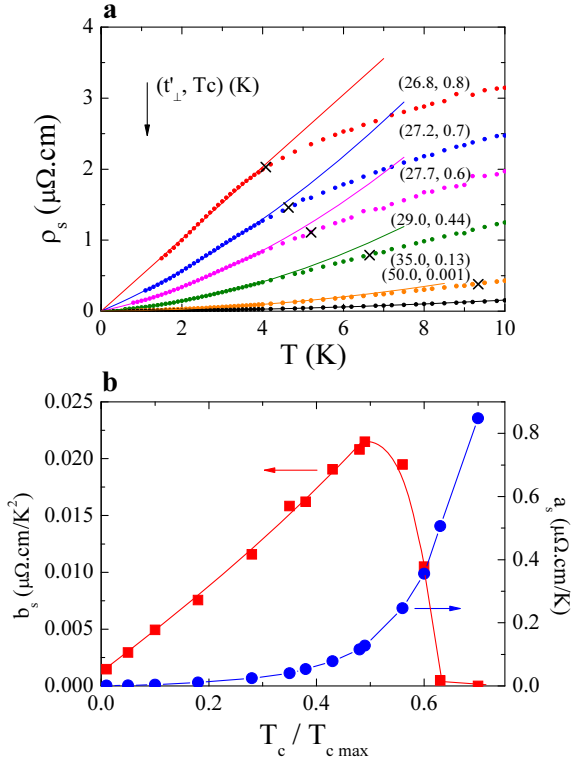
Fig. 10. (Color online) (a) Temperature dependence of the calculated resistivity from the singular part of the self-energy for the quasi-one-dimensional electron gas model in the superconducting sector. The continuous line is a fit to the expression (2) in the interval 4 K > T > 1 K and crosses refer to the scale T_0 below which the polynomial form prevails. (b) Variation of the linear and quadratic coefficients a_s and b_s obtained from the fit of ρ_s in (a) as a function of T_c/T_{cmax}. The lines between the points are guides to the eye.

frequency. The expression of the calculated resistivity $\rho_s(T) = \sigma_s^{-1}(T)$, can be rewritten as $\rho_s(T) = \rho_0\tau_0/\langle\tau_{k_\perp}\rangle$ using the Drude formula for the residual resistivity $\rho_0 = 4\pi/(\omega_p^2\tau_0)$ and the elastic scattering time τ_0. The value of ρ_0 (in $\mu\Omega$ cm) can be fixed to the experimental data for $(TMTSF)_2PF_6$ (Sect. 3.2.1) and $(TMTSF)_2ClO_4$ (Sect. 3.2.2), letting the normalization time scale τ_0 as a parameter to be fixed. However, there is a common discrepancy as to the actual value of τ_0 in these materials [43,58,59]. Taking for example $\rho_0 \sim 3$ $\mu\Omega$ cm, as a typical range of residual resistivity above P_c (Fig. 3), and the electron density of $n \simeq 1.4 \times 10^{21}$ cm^{-3} [60], one finds $\tau_0 \approx 0.8 \times 10^{-12}$ s using the Drude formula. On the other hand, the analysis of both the Drude peak in optical conductivity near T_c [58] and the non-magnetic pair breaking effect on T_c [26] yield $\tau_0 \sim 10^{-11}$ s, a significantly larger value. In the following we shall take $\tau_0 = 2.5 \times 10^{-12}$ s, a value that falls within the above bracket and leads to an amplitude of calculated resistivity in the range of observed values for $\rho_a - \rho_0$ above T_c (Fig. 3).

The calculated temperature dependence of the parallel resistivity $\rho_s(T) = 1/\sigma_s(T)$ is shown in Figure 10a for different amplitudes of the antinesting parameter $t'_\perp$, which

correspond to different values of the ratio T_c/T_{cmax}. Not shown in the Figure are the cases where $t'_\perp \sim t'^*_\perp$, namely close to the critical 'pressure' in the phase diagram. In this domain the fluctuations, for the most part antiferromagnetic, become sufficiently pronounced to induce critical scattering and an insulating behavior at low temperature, despite the presence of a superconducting ground state – the paraconductive contribution to conductivity being excluded of the present calculations. While reminiscent of the reentrant region of the actual phase diagram close to P_c (Fig. 1a), this behavior signals the flow to strong coupling.

As $t'_\perp$ grows apart from $t'^*_\perp$, the resistivity becomes metallic at low temperature. It drops with an inward curvature down to the temperature scale T_0, below which it shows a downtrend toward zero. This is displayed in Figure 10a down to the beginning of criticality close T_c where the RG procedure is stopped. Contrary to what is expected for a Fermi liquid, however, the resistivity is rather well described by the polynomial form

$$\rho_s(T) \approx a_sT + b_sT^2, \tag{2}$$

within the interval $T_c \lesssim T < T_0$, which falls within the Curie-Weiss domain of spin correlations discussed previously in the framework of NMR relaxation. At the lowest $t'_\perp$ shown in Figure 10a (26.8 K or $T_c \simeq 0.8$ K), the interval is bound from below by the onset of the superconducting critical fluctuations in the vicinity of T_c and extends up to $T_0 \approx 4$ K (cross in Fig. 10a). At that $t'_\perp$, the temperature dependence is essentially described by a linear term with $b_s \approx 0$ (Fig. 10b). The existence of linearity is the consequence of the scattering of electrons on prominent antiferromagnetic fluctuations, though strongly mixed with Cooper SCd pairing. These fluctuations are peaked at frequencies smaller than the temperature and as bosonic excitations, their coupling to electrons in two dimensions is known to yield a scattering rate $\tau_{k_\perp}^{-1} \sim T\xi$, which is essentially linear in temperature when the correlation length ξ becomes temperature independent. This is the case of the Curie-Weiss domain where $\tau_{k_\perp}^{-1} \sim T$ at $T \ll \Theta$. The RG results presented here are compatible with this limit.

As $t'_\perp$ further increases, however, one gradually departs from this limit. The temperature domain where the resistivity follows the polynomial form (2) expands due to the growth of T_0 and the drop of T_c. While the linear term persists far from $t'^*_\perp$, the a_s coefficient steadily declines with the strength of antiferromagnetic correlations and T_c (Fig. 10). The decrease of $a_s \sim T_c^2$ approximately follows the square of the critical temperature showing that both quantities are closely related (see Fig. 10b). A distinct feature that comes out of the RG calculations of Figure 10a is the emergence of a b_sT^2 – Fermi liquid – term that accompanies the drop of a_s within the same temperature interval. The b_s factor first rises from zero, reaches a maximum to finally decrease and level off toward small values at large $t'_\perp$ or vanishing T_c (Fig. 10b). This interplay between the two terms is indicative of a progressive shift of the fluctuation spectral weight to frequency scales higher than temperature. The stiffening of

fluctuation frequency with respect to T yields favorable conditions for establishing a Fermi liquid component [61].

Interestingly, the overall amplitude of resistivity follows a trend similar to T_c and vanishes at large $t'_\perp$, according to Figure 10a. While this behavior adheres with the one found in experiments for the strength of the inelastic contribution $\Delta\rho_a = \rho_a - \rho_0$ close to T_c, as shown in Figure 3 and in reference [3], it differs well above this scale where a sustained T^2 variation of resistivity is experimentally found. It turns out, however, that the RG self-energy calculations considered so far only include contributions of the singular electron-hole and electron-electron scattering channels. The RG procedure actually neglects all pieces of residual scattering that in principle also yield a T^2 term for the quasi-particle decay rate and resistivity – a $T^2 \ln T$ term to be exact in strictly two dimensions [40,41]. The latter contribution eventually takes over and dominates as the temperature is raised and antiferromagnetic correlations decrease enough in amplitude. The situation is similar to the one found in the description of NMR experiments (e.g. inset of Fig. 8, and Refs. [6,62]), where non singular spin fluctuations, uniform to be specific, give rise to a Korringa like temperature dependence for the nuclear spin relaxation rate $((T_1T)^{-1} \propto \chi^2(\mathbf{q} = 0))$ reference [8]. As the temperature grows, this Fermi liquid contribution ultimately overcomes the low-T enhancement of T_1^{-1} coming from antiferromagnetism.

The regular contribution to the scattering rate can be in first approximation be considered decoupled from the singular part of the self-energy – an approximation that has its limitations as we will see. It can thus be added to the expression (2), according to the usual rule $\rho \rightarrow \rho_s(T) + b_r T^2$ – dropping the 2D $\ln T$ correction, which has been assumed to be cut off by the transverse hopping term in the third direction. We shall fix the coefficient b_r by adjusting the calculated ρ to the experimental values of $\Delta\rho_a(15\,\text{K})$ obtained at 15 K for (TMTSF)$_2$PF$_6$ and (TMTSF)$_2$ClO$_4$ at different pressures or T_c (Figs. 3 and 4). The resulting trace of the calculated resistivity versus temperature is shown in Figure 11 for different $t'_\perp$ (or T_c) in the case of (TMTSF)$_2$PF$_6$ (Fig. 11a) and (TMTSF)$_2$ClO$_4$ (Fig. 11b). The calculated data points have been fitted to the polynomial form $\rho(T) = aT + bT^2$ in the interval $1\,\text{K} < T < 4\,\text{K}$ (continuous curves in Fig. 10b), from which the variation of the linear a and b coefficients with the ratio T_c/T_{cmax} can be extracted and compared to experiments.

The variation of the linear coefficient a against the ratio T_c/T_{cmax} is given in Figure 12a and compared with experimental results of Section 4.1.1 for the PF$_6$ and ClO$_4$ salts[1]. It is clear here that the only contribution to the linear term comes from the singular part, so that $a \approx a_s$ and essentially coincides with the one of Figure 10b. Thus compared to the values extracted for both materials on
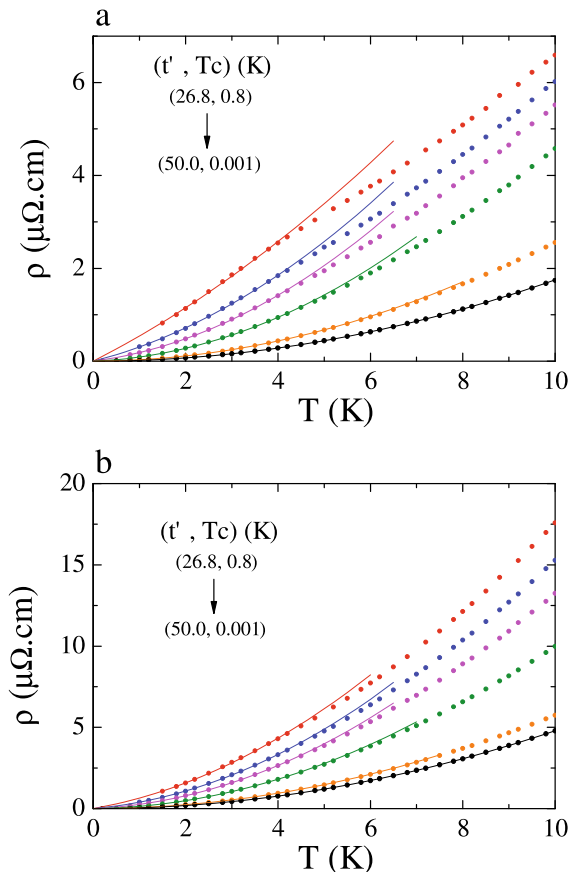
Fig. 11. (Color online) Temperature dependence of the calculated resistivity including a residual Fermi liquid part for the (TMTSF)$_2$PF$_6$ (a) and (TMTSF)$_2$ClO$_4$ (b) salts. The continuous lines correspond to a polynomial fit to $\rho(T) = aT + bT^2$ in the interval $4 > T > 1$ K.

experimental grounds, the calculated a coefficient shows a nearly quadratic variation with T_c, which is stronger than found experimentally. The present theory, however, captures the progressive decay of the linear coefficient under 'pressure'. The change is staggered over the entire domain of variation of $t'_\perp$ where T_c differs noticeably from zero. The fact that a sizable amplitude of a is not just confined to the very close proximity of $t'^*_\perp$ or P_c on the pressure scale, contrasts with what is commonly expected near a quantum critical point [63,64]. This reveals that the anomalous source of scattering for electrons is only gradually suppressed under 'pressure', leading to a broadened interval of pressure over which quantum critical behavior can survive. Extended criticality is attributable to the presence of Cooper pairing, which remains singular and interferes positively with antiferromagnetism; this provides the link between the linear resistivity and T_c.

We now consider the variation of the Fermi liquid coefficient b as a function of T_c/T_{cmax}, which is shown in Figure 12b for the PF$_6$ salt and in Figure 12c for ClO$_4$. In the case of PF$_6$, this regular Fermi liquid behavior at high temperature is not strongly pronounced which lets the singular contribution of Figure 10b showing through the variation of b with T_c. A maximum of b at intermediate
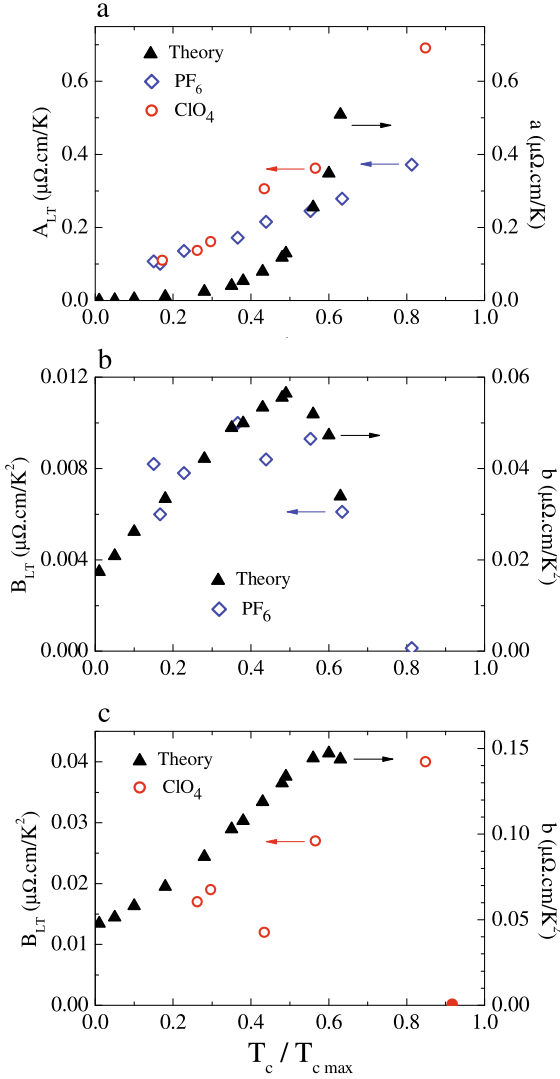
Fig. 12. (Color online) Variation of the calculated linear resistivity coefficient a (a), and the Fermi liquid coefficient b for $(TMTSF)_2PF_6$ (b) and $(TMTSF)_2ClO_4$ (c) as a function of the ratio T_c/T_{cmax} (full triangles). The open diamonds (open circles) correspond to the experimental data of $(TMTSF)_2PF_6$ ($(TMTSF)_2ClO_4$)(Sect. 4.1.2). The experimental point at T_c/T_{cmax}=0.91 for $(TMTSF)_2ClO_4$ refers to the ambient pressure data in Figure 2.

T_c is thus found, an important result that is manifest in $(TMTSF)_2PF_6$. In the case of $(TMTSF)_2ClO_4$, the Fermi liquid term at high temperature is about three times stronger, leading to a larger regular b_rT^2 contribution. This removes some weight of the Fermi liquid b_sT^2 component coming from the singular term, and as a result, the maximum in b is scarcely seen, being masked for the most part by the contribution of the regular contribution.

6 Conclusion

In summary, this work reports a careful investigation of the metallic phase of $(TMTSF)_2PF_6$ and $(TMTSF)_2ClO_4$ carried out under pressure which confirms the role played by high pressure controlling the size of electron correlations and in turn the stability of superconductivity in these compounds. However, this new study is pointing out a salient difference between the diagrams of these two superconductors. An important control parameter of superconductivity in $(TMTSF)_2X$ is also the value of the elastic electron life time. Such a lifetime is governed in $(TMTSF)_2ClO_4$ by the level of residual non magnetic impurities originating from the imperfect anion ordering under high pressure conditions. The possibility to achieve a large number of high pressure runs using a single sample has enabled an exhaustive and quantitative analysis of longitudinal transport experiments in the temperature regime 0–20 K in a wide pressure regime. Processing the transport data using a sliding fit procedure in temperature according to a second order polynomial form, $\rho(T) = \rho_0 + AT + BT^2$ and T dependent prefactors, reveals two temperature domains.

A high temperature domain ($T \approx 20$ K) in which the regular T^2 electron-electron Umklapp scattering obeys a Kadowaki-Woods law. A low temperature regime ($T < 8$ K) in which the scattering of carriers against antiferromagnetic fluctuations provides for $(TMTSF)_2PF_6$ a purely linear T dependent contribution [3].

This linear in temperature component of transport is connected to the intrinsic pressure dependence of T_c which is controlled by pressure while an additional control parameter of T_c is given by the residual anion disorder in the case of $(TMTSF)_2ClO_4$. In both compounds a correlated behavior exists between the linear term of transport and the extra nuclear spin-lattice relaxation due to antiferromagnetic fluctuations.

In $(TMTSF)_2PF_6$, where the temperature dependence of the resistivity is likely cleaner than for $(TMTSF)_2ClO_4$ since it is free from the pollution of the ClO_4 anions ordering over a wide T regime, a *purely* linear in T dependence ($B \to 0$) extending up to 8 K supports the vanishing of the regular part of the quadratic scattering but does not imply the opening of a pseudo gap in the charge sector. The theoretical treatment of fluctuations in the case of channel mixing will require additional work.

Other studies of metallic and superconducting phases of these compounds would be highly desirable in the future, in particular a reinvestigation of the far-infrared properties, additional NMR work under pressure in both compounds and a detailed investigation of transport in the vicinity of the critical pressure in $(TMTSF)_2PF_6$.

We have compared in some details the experimental data to the predictions of the two-loop scaling theory for the resistivity, as it can be derived from the quasi-particle scattering rate within the Boltzmann picture. A low temperature linear term for resistivity emerges naturally from the theory; its amplitude peaks near the critical point and is followed by a gradual decay extending over the entire range of pressure where a – d-wave – superconducting T_c differs from zero. This remarkable feature co-occurs with another one, namely the low temperature development of Fermi liquid scattering whose pressure dependence is for the most part opposed to the one of the linear component

of resistivity. Both results are finding a favorable echo in a material like (TMTSF)$_2$PF$_6$, and to a large extent in (TMTSF)$_2$ClO$_4$ as well.

The correlation between linear resistivity and T_c can definitely be regarded as another important result of the theory. It supplies some basic microscopic insight on the behavior of electron scattering in the presence of antiferromagnetic fluctuations and Cooper pairing, a long-established problem in unconventional superconductors. In the quasi-one dimensional electron gas these two channels of correlations are intrinsically interdependent, which is systematically taken into account within scaling theory. This compound pairing turns out to be of crucial importance in matching the pressure range of linear resistivity to the one of T_c. The view developed in this work about electrical resistivity proves to be internally consistent with the previous analysis made in the context of the nuclear relaxation and the phase diagram using the same approach. This gives important additional support to the model proposed.

References

1. D. Jérome, A. Mazaud, M. Ribault, K. Bechgaard, J. Phys. Lett. (Paris) **41**, L95 (1980), open archive on HAL http://hal.archives-ouvertes.fr/
2. K. Bechgaard, K. Carneiro, M. Olsen, F.B. Rasmussen, Phys. Rev. Lett. **46**, 852 (1981)
3. N. Doiron-Leyraud, P. Auban-Senzier, S. René de Cotret, C. Bourbonnais, D. Jérome, K. Bechgaard, L. Taillefer, Phys. Rev. B **80**, 214531 (2009)
4. N. Doiron-Leyraud, P. Auban-Senzier, S. René de Cotret, C. Bourbonnais, D. Jérome, K. Bechgaard, L. Taillefer, Physica B **405**, S265 (2010), *Proceedings of ISCOM 2009*, arXiv.org:0912.2049
5. N. Doiron-Leyraud, P. Auban-Senzier, S. René de Cotret, C. Bourbonnais, D. Jérome, K. Bechgaard, L. Taillefer, arXiv.org:0905.0964
6. P. Wzietek, F. Creuzet, C. Bourbonnais, D. Jérome, K. Bechgaard, P. Batail, J. Phys. I France **3**, 171 (1993), open archive on HAL http://hal.archives-ouvertes.fr/
7. S.E. Brown et al., in *The Physics of Organic Superconductors and Conductors*, edited by A. Lebed (Springer Series in Materials Sciences, Heidelberg, 2008), p. 76
8. C. Bourbonnais, A. Sedeki, Phys. Rev. B **80**, 085105 (2009), arXiv.org:0904.2858
9. S.S.P. Parkin, J. Voiron, R.L. Greene, Mol. Cryst. Liq. Cryst. **119**, 33 (1985)
10. S. Tomić, D. Jérome, D. Mailly, M. Ribault, K. Bechgaard, J. Phys. **44**, C3–1075 (1983)
11. N. Joo, C. Pasquier, P. Auban-Senzier, D. Jérome, Eur. Phys. J. B **40**, 43 (2004)
12. S. Tomić, D. Jérome, D. Mailly, M. Ribault, K. Bechgaard, J. Phys. **44**, C3, 1083 (1983), open archive on HAL http://hal.archives-ouvertes.fr/
13. T. Ishiguro et al., J. Phys. **44**, C3–831 (1983), open archive on HAL http://hal.archives-ouvertes.fr/
14. R. Duprat, C. Bourbonnais, Eur. Phys. J. B **21**, 219 (2001)
15. J.C. Nickel, R. Duprat, C. Bourbonnais, N. Dupuis, Phys. Rev. B **73**, 165126 (2006)
16. C. Bourbonnais, L.G. Caron, Europhys. Lett. **5**, 209 (1988)
17. V.J. Emery, R. Bruinsma, S. Barisić, Phys. Rev. Lett. **48**, 1039 (1982)
18. W. Wu et al., Phys. Rev. Lett. **94**, 097004 (2005)
19. A. Sedeki, D. Bergeron, C. Bourbonnais, Physica B **405**, S89 (2010), *Proceedings of ISCOM 2009*
20. K. Bechgaard, C.S. Jacobsen, K. Mortensen, H.J. Pedersen, N. Thorup, Solid State Commun. **33**, 1119 (1979)
21. I.R. Walker, Rev. Sci. Instr. **70**, 3402 (1999)
22. T. Vuletić, P. Auban-Senzier, C. Pasquier, S. Tomić, D. Jérome, M. Héritier, K. Bechgaard, Eur. Phys. J. B **25**, 319 (2002)
23. N. Kang, B. Salameh, P. Auban-Senzier, D. Jérome, C.R. Pasquier, S. Brazovskii, Phys. Rev. B. **81**, R100509 (2010)
24. M. Ribault, G. Benedek, D. Jérome, K. Bechgaard, J. Phys. Lett. Paris **41**, L–397 (1980)
25. S. Yonezawa, Y. Maeno, P. Auban-Senzier, C. Pasquier, K. Bechgaard, D. Jérome, Phys. Rev. Lett. **100**, 117002 (2008)
26. N. Joo, P. Auban-Senzier, C. Pasquier, D. Jérome, K. Bechgaard, Eur. Phys. Lett. **72**, 645 (2005)
27. P. Auban-Senzier et al. (2010), to be published
28. J.P. Pouget et al., J. Phys. **44**, C3–969 (1983), open archive on HAL http://hal.archives-ouvertes.fr/
29. J.P. Pouget, G. Shirane, K. Bechgaard, J.M. Fabre, Phys. Rev. B (1983)
30. F. Pesty, P. Garoche, A. Moradpour, Mol. Cryst. Liq. Cryst. **119**, 251 (1985)
31. S. Kagoshima et al., Solid State Commun. **46**, 867 (1983)
32. J.P. Pouget et al., J. Phys. Soc. Jpn **59**, 2036 (1990)
33. K. Murata, L. Brossard, R.C. Lacoe, M. Ribault, D. Jérome, K. Bechgaard, A. Moradpour, Mol. Cryst. Liq. Cryst. **119**, 245 (1985)
34. F. Creuzet, D. Jérome, A. Moradpour, Mol. Cryst. Liq. Cryst. **119**, 297 (1985)
35. F. Guo et al., J. Phys. Soc. Jpn **67**, 3000 (1998)
36. W. Kang, S.T. Hannahs, P.M. Chaikin, Phys. Rev. Lett. **70**, 3091 (1993)
37. P. Garoche, R. Brusetti, K. Bechgaard, Phys. Rev. Lett. **49**, 1346 (1982)
38. N. Matsunaga et al., J. Low Temp. Phys. **117**, 1735 (1999)
39. H.J. Schulz, D. Jérome, M. Ribault, A. Mazaud, K. Bechgaard, J. Phys. Lett. **42**, L (1981), open archive on HAL http://hal.archives-ouvertes.fr/
40. L.P. Gorkov, M. Mochena, Phys. Rev. B **57**, 6204 (1998)
41. C. Hodges, H. Smith, J.W. Wilkins, Phys. Rev. B **4**, 302 (1971)
42. B. Welber, P.E. Seiden, P.M. Grant, Phys. Rev. B **118**, 2692 (1978)
43. D. Jérome, H.J. Schulz, Adv. Phys. **31**, 299 (1982)
44. J.R. Cooper, L. Forró, B. Korin-Hamzić, K. Bechgaard, A. Moradpour, Phys. Rev. B **33**, 6810 (1986)

45. B. Korin-Hamzic, L. Forro, J.R. Cooper, K. Bechgaard, Phys. Rev. B **38**, 11177 (1986)
46. S. Tomič, J.R. Cooper, W. Kang, D. Jérome, K. Maki, J. Phys. I France **1**, 1603 (1991), open archive on HAL http://hal.archives-ouvertes.fr/
47. G. Creuzet, J.R. Cooper, F. Creuzet, D. Jerome, A. Moradpour, J. Phys. Lett. **46**, L–1133 (1985), open archive on HAL http://hal.archives-ouvertes.fr/
48. K. Kadowaki, S.B. Woods, Solid State Commun. **58**, 507 (1986)
49. B.J. Powell, private communication
50. H. Niedoba, H. Launois, D. Brinkmann, H.U. Keller, J. Phys. Lett. **35**, L–251 (1974), open archive on HAL http://hal.archives-ouvertes.fr/
51. N. Miljak, J.R. Cooper, K. Bechgaard, J. Phys. **44**, C3–893 (1983), open archive on HAL http://hal.archives-ouvertes.fr/
52. N. Miljak, J.R. Cooper, Mol. Cryst. Liq. Cryst. **119**, 141 (1985)
53. L. Ducasse, A. Abderraba, J. Hoarau, M. Pesquer, B. Gallois, J. Gaultier, J. Phys. C **39**, 3805 (1986)
54. D. Le Pévelen, J. Gaultier, Y. Barrans, D. Chassau, F. Castet, L. Ducasse, Eur. Phys. J. B **19**, 363 (2001)
55. F. Creuzet, C. Bourbonnais, L.G. Caron, D. Jérome, K. Bechgaard, Synth. Met. **19**, 289 (1987)
56. J. Shinagawa, Y. Kurosaki, F. Zhang, C. Parker, S.E. Brown, D. Jérome, Phys. Rev. Lett. **98**, 147002 (2007)
57. C. Bourbonnais, F. Creuzet, D. Jérome, K. Bechgaard, A. Moradpour, J. Phys. Lett. France **45**, L755 (1984), open archive on HAL http://hal.archives-ouvertes.fr/
58. H.K. Ng, T. Timusk, K. Bechgaard, J. Phys. **44**, C3–867 (1983), open archive on HAL http://hal.archives-ouvertes.fr/
59. M. Dressel, A. Schwartz, G. Grüner, L. De Giorgi, Phys. Rev. Lett. **77**, 398 (1996)
60. J. Moser, J.R. Cooper, D. Jérome, B. Alavi, S.E. Brown, K. Bechgaard, Phys. Rev. Lett. **84**, 2674 (2000)
61. Y. Vilk, A.-M. Tremblay, J. Phys. I France (1997), open archive on HAL http://hal.archives-ouvertes.fr/
62. C. Bourbonnais, P. Wzietek, D. Jérome, F. Creuzet, K. Bechgaard, P. Batail, Phys. Rev. Lett. **62**, 1532 (1989)
63. A. Abanov, A.V. Chubukov, J. Schmalian, Adv. Phys. **52**, 119 (2003)
64. T. Moriya, Y. Takahashi, K. Ueda, J. Phys. Soc. Jpn **59**, 2905 (1990)